


Allee thresholds and basins of attraction in a predation model with double Allee effect

Dana Contreras Julio | Pablo Aguirre 

Departamento de Matemática,
Universidad Técnica Federico Santa
María, Casilla 110-V, Valparaíso, Chile

Correspondence

Pablo Aguirre, Departamento de
Matemática, Universidad Técnica
Federico Santa María, Casilla 110-V,
Valparaíso, Chile.
Email: pablo.aguirre@usm.cl

Communicated by: I. Sevostianov

Funding information

CONICYT-FONDECYT, Grant/Award
Number: 11150306; Proyecto Basal CMM
Universidad de Chile

MSC Classification: 92D25; 34C45;
37M20; 37C29

We investigate the nature of Allee thresholds and basins of attraction in a predation model with double Allee effect in the prey and a competition behaviour in the predator. From a mathematical perspective, this implies to find and characterise the corresponding basin boundaries in phase space. This is typically a major challenge since the objects that act as boundaries between 2 different basins are invariant manifolds of the system, which may also undergo topological changes at bifurcations. For this goal, we make an extensive use of analytical tools from dynamical systems theory and numerical bifurcation analysis and determine the full bifurcation diagram. Local bifurcations include saddle-node, transcritical and Hopf bifurcations, while global phenomena include homoclinic bifurcations, heteroclinic connections, and heteroclinic cycles. We identify the Allee threshold to be either a limit cycle, a homoclinic orbit, or the stable manifold of an equilibrium. This strategy based on bifurcation and invariant manifold analysis allows us to identify the mathematical mechanisms that produce rearrangements of separatrices in phase space. In this way, we give a full geometrical explanation of how the Allee threshold and basins of attraction undergo critical transitions. This approach is complemented with a study of the dynamics near infinity. In this way, we determine the conditions such that the basins of attraction are bounded or unbounded sets in phase space. All in all, these results allow us to show a complete description of phase portraits, extinction thresholds, and basins of attraction of our model under variation of parameters.

KEYWORDS

Allee effect, Allee threshold, basin boundaries, bifurcation analysis, invariant manifolds

1 | INTRODUCTION

One of the key questions in population dynamics is to determine conditions for survival (or extinction) of populations. From the mathematical viewpoint, this corresponds to identify the basins of attraction of the relevant attracting sets in the system, that is, the set of all initial conditions that converge to a particular attractor in the long term, whether this is an equilibrium point, a periodic orbit, or even a strange attractor.¹ More formally, if Φ^t defines the time evolution of the dynamics of a particular model, the basin of attraction $B(\mathbf{A})$ of an attracting set \mathbf{A} is defined as

$$B(\mathbf{A}) = \bigcup_{t \leq 0} \Phi^t(U),$$

where $U \subset \mathbb{R}^2$ is any open neighbourhood of \mathbf{A} such that $\Phi^t(U) \subset U$ ($\forall t \geq 0$) and $\bigcap_{t \geq 0} \Phi^t(U) = \mathbf{A}$.^{1,2}

The characterisation of the corresponding basin boundaries $\partial\mathcal{B}(\mathbf{A})$ is of special interest when there is more than 1 possible final outcome for populations, ie, the system has more than 1 coexisting attractor. The key to distinguish between the basins of 2 different attractors and their common boundary lies in the identification of a saddle object (a saddle equilibrium or a saddle periodic orbit, for instance). In the case of a saddle point \mathbf{x}^* , this saddle equilibrium has an associated stable manifold defined as the set

$$W^s(\mathbf{x}^*) = \{ \mathbf{x} \in \mathbb{R}^n | \Phi^t(\mathbf{x}) \rightarrow \mathbf{x}^* \text{ as } t \rightarrow \infty \},$$

which consists of points that converge to the saddle in positive time under the flow Φ^t (the stable manifold of a saddle periodic orbit can be defined much in the same way).^{1,2} Typically, the stable manifold $W^s(\mathbf{x}^*)$ is the mathematical object that separates the basins of 2 different attractors. Hence, to characterise any particular basin of attraction, one needs to find the corresponding stable manifolds of saddle objects in phase space that form its basin boundary; see, for instance, Aguirre et al.³⁻⁵ In the case of population models, this analysis allows one to give specific conditions for extinction and survival.

The computation of global stable and unstable manifolds is a major challenge. Indeed, in general, these invariant manifolds cannot be calculated analytically as global objects in phase space, and, hence, one has to approximate them with numerical techniques.⁶ Moreover, stable manifolds can undergo critical rearrangements under parameter variation.^{1,2,4,5} These reconfigurations of stable manifolds can produce dramatic transitions in the basins they separate.³ Hence, a combination of stable manifold analysis and bifurcation theory emerges as a necessary strategy to understand how the phase space is partitioned by different basins of attraction.

1.1 | The model with double Allee effect

In this work, we consider a predator-prey model with a strong double Allee effect⁷⁻⁹ on the prey population with the specific aim to shed light on the conditions for extinction and survival of the populations. The model is given as the following system of differential equations:

$$\mathbf{X} : \begin{cases} \dot{x} = \frac{rx}{x+n} \left(1 - \frac{x}{k}\right) (x - m) - qxy, \\ \dot{y} = sxy - dy - cy^2. \end{cases} \quad (1)$$

Here, the population sizes of the prey and predators are given by $x(t)$ and $y(t)$, respectively, with $t \geq 0$. We study solutions of (1) in the first quadrant, that is, $(x(t), y(t)) \in \Omega = \{(x, y) \in \mathbb{R}^2 | x \geq 0, y \geq 0\}$. Parameters $r > 0$ and $s > 0$ are the intrinsic growth rate of biotic potential of the population x and y , respectively; $k > 0$ is the prey carrying capacity; $q > 0$ is the maximum per capita consumption rate of predators; and $d > 0$ is the predator natural mortality rate. On the other hand, $c > 0$ is a competition rate among predators. Hence, the term $-cy^2$ can also denote the existence of a density-dependent death rate given by the factor $-cy$.¹⁰ See also Bazykin¹¹ and Murray¹² and the references therein for more details. Finally, parameters m and n are related to the double Allee effect in the model and will be explained below.

Model (1) presents Allee effect on the prey population.^{7-10,13} This phenomenon is characterised by a tendency of the population growth rate to decrease under some minimum critical level.¹⁴ Typically, a population with Allee effect faces difficulties to grow from low densities and avoid extinction. Indeed, the population growth rate may become negative indicating the existence of an extinction threshold—commonly known as the Allee threshold—that the population has to overcome to survive and avoid extinction.¹⁴⁻¹⁶ Among the causes that may generate an Allee effect on a population are the difficulty of finding fertile mates or a low social interaction.^{8,17,18} Other causes include Allee effects generated by predation¹⁹⁻²³: When at low densities, a population may show difficulties to better defend or hide from a predator.²⁴⁻²⁷

In certain cases, 2 or more Allee effects can impact simultaneously on a single population in a phenomenon that has been called a double Allee effect.^{17,28,29} In (1), the double Allee effect is given by the term $A(x) = 1 - \frac{m+n}{x+n}$, which multiplies the expression of classic logistic growth in the prey equation. This form for $A(x)$ was proposed in Boukal and Berec³⁰ and accounts for a higher extinction rate on small populations than in other modelling approaches; hence, the term $A(x)$ fits nicely with the concept of 2 simultaneous Allee effects on the same population. The 2 Allee effects in $A(x)$ can be interpreted by rewriting it as the product of 2 factors $A(x) = \frac{1}{x+n} (x - m)$, each one representing an independent Allee effect. This is the way the Allee function $A(x)$ is presented in Equation (1). The first factor $(x - m)$, where $0 < m < k$ throughout this paper, is the most familiar mathematical expression to indicate a multiplicative strong Allee effect; see Bazykin¹¹ and Aguirre³¹ and the references therein. In particular, for an isolated population, parameter m is often interpreted as an Allee threshold, ie, the minimum viable population density that guarantees long-term non-extinction. On the other hand,

the second factor, $\frac{1}{x+n}$, represents the presence of a second Allee effect due to a fraction $n > 0$ of the population being nonfertile.^{32,33} As the number of sterile members n of the population is increased, the Allee function $A(x)$ decreases, and hence, the population has greater difficulties to grow.

The Allee effect and its consequences for ecology and conservation have been the subject of investigations for decades; see Lidicker Jr⁹ and Stephens et al³⁴ and the references therein. However, as far as we know, only a few works have addressed the subject of multiple Allee effects. For instance, González-Olivares et al^{29,33} use the same expression for $A(x)$ as in (1) with the aim of comparing their properties to predation models with simple Allee effect. In turn, our goal in this work is to extend the analysis to include an additional phenomenon of competition among the predators and to address the question of what are the possible Allee thresholds in the model. Indeed, some of the most important recent advances on population models with Allee effect focus on stability of equilibrium points, the number of limit cycles, and local bifurcation analysis; see, for instance, Aguirre et al³⁵ and González-Olivares et al.³⁶⁻³⁸ However, to the best of our knowledge, only a few works have investigated the features of Allee thresholds and basins of attraction and their relation to bifurcations under system parameters in predation models,^{6,39-41} let alone in the presence of multiple Allee effects. This is a relevant challenge. In a 2-dimensional model such as (1), the mathematical object that corresponds to the Allee threshold is the (1-dimensional) boundary of the basin of the origin. In this work, for the specific example of (1), we identify 3 possible scenarios: the Allee threshold either corresponds to (1) the stable manifold of a distinguished equilibrium in phase space, (2) to a limit cycle, (3) or to a homoclinic orbit, ie, an orbit that connects a saddle equilibrium in both forward and backward time.

By means of analytical tools from dynamical systems theory¹ and numerical bifurcation analysis,^{2,42} we determine the bifurcation diagram including local and global bifurcations. We find 3 codimension-2 points that act as organisation centres for the dynamics. Curves of homoclinic, heteroclinic, Hopf, saddle-node, and transcritical bifurcations emanate from these points and, thus, subdivide the parameter space into several open regions with characteristic phase portraits. This allows us to pinpoint the mathematical mechanisms in (1) that produce rearrangements of the stable manifolds involved. In this way, we give a full geometrical explanation of how the Allee threshold undergoes critical transitions. This bifurcation approach is complemented with a study of the dynamics near infinity. In this way, we determine the conditions such that the basins of attraction are bounded or unbounded sets in phase space. All in all, these results allow us to show a complete description of phase portraits, extinction thresholds, and basins of attraction of (1) under variation of parameters.

1.2 | Preliminaries

In preparation for the analysis, we transform (1) into a polynomial system. This is achieved by the change of coordinates and time rescaling,

$$(x, y, t) \mapsto \left(kx, \frac{y}{q}, (x+n)t \right), \quad (2)$$

followed by the change of parameters,

$$(r, n, k, q, s, c, d, m) \mapsto (r, N, k, q, S, C, d, M) := \left(r, \frac{n}{k}, k, q, sk, \frac{c}{q}, d, \frac{m}{k} \right). \quad (3)$$

The transformations (2) and (3) on system (1) define a polynomial system in Ω given by

$$\mathbf{Y} : \begin{cases} \dot{x} = x[r(1-x)(x-M) - y(x+N)], \\ \dot{y} = y(x+N)(Sx - d - Cy). \end{cases} \quad (4)$$

The advantage of this preliminary procedure is that (4) is a polynomial system that is equivalent to (1) in the sense that orbits of system \mathbf{X} are mapped onto orbits of system \mathbf{Y} in a biunique way preserving the time orientation of solutions.^{1,2} Moreover, (4) has the reduced vector of 6 (positive) parameters $(r, N, S, d, C, \text{ and } M)$, which also makes it easier to analyse. Notice that $0 < M < 1$. Hence, for the sake of clarity, we denote the new space of parameters as $\Lambda := \mathbb{R}_+^5 \times]0, 1[$, ie, the product space of \mathbb{R}_+^5 and the open interval $]0, 1[$.

The structure of this paper is the following: In Section 2, we study the behaviour of the system near infinity and prove that the solutions of (4) are bounded and non-negative. Section 3 deals with the stability of equilibrium points and the local bifurcations involved. The analysis of global bifurcations and basins of attraction is conducted in Section 4. Finally, a discussion of the results is given in Section 5.

2 | THE SOLUTIONS ARE BOUNDED AND NON-NEGATIVE

From now on, it is more convenient to treat \mathbf{Y} as a vector field in Ω . The restriction of \mathbf{Y} along the x -axis is given by $\mathbf{Y}(x, 0) = (xr(1-x)(x-M), 0)^\top$, which defines a strictly horizontal flow. Similarly, along the y -axis, one has $\mathbf{Y}(0, y) = (0, -yN(Cy+d))^\top$, which is strictly vertical. Hence, the vector field \mathbf{Y} is invariant along the coordinate axes. Thus, every orbit of \mathbf{Y} in the interior of the first quadrant remains inside this open region. Hence, solutions starting in the first quadrant remain non-negative. Moreover, it is easy to see that no trajectory along the coordinate axes converges to infinity in forward time.

Our aim now is to prove that no trajectory in the interior of the first quadrant converges to infinity in forward time. To do so, it suffices to study the behaviour of solutions in \mathbf{Y} at infinity as $x, y \rightarrow \infty$ by means of a Poincaré compactification.^{31,35}

To study the solutions as $x \rightarrow \infty$, we consider the transformation of coordinates and time rescaling given by

$$(x, y, t) \mapsto \left(\frac{1}{\hat{u}}, \frac{\hat{v}}{\hat{u}}, \hat{u}^2 t \right), \quad \hat{u} > 0, \hat{v} \geq 0. \quad (5)$$

In this way, transformation (5) defines the following system:

$$\mathbf{Y}_{\hat{u}\hat{v}} : \begin{cases} \dot{\hat{u}} = \hat{u} [r(\hat{u}-1)(M\hat{u}-1) + \hat{v}(N\hat{u}+1)] ; \\ \dot{\hat{v}} = \hat{v} [r(\hat{u}-1)(M\hat{u}-1) + (N\hat{u}+1)(S-d\hat{u} + \hat{v} - C\hat{v})] . \end{cases} \quad (6)$$

Orbits of \mathbf{Y} at infinity as $x \rightarrow \infty$ can be studied by investigating the dynamics of $\mathbf{Y}_{\hat{u}\hat{v}}$ along the invariant line $\hat{u} = 0$ for $\hat{v} \geq 0$. The origin $\mathbf{0}_{\hat{u}\hat{v}} = (0, 0)$ is always an equilibrium of (6), and (if $C > 1$) we also have $q_c = \left(0, \frac{r+s}{C-1}\right)$. The Jacobian matrices associated to these equilibria are

$$D\mathbf{Y}_{\hat{u}\hat{v}}(\mathbf{0}_{\hat{u}\hat{v}}) = \begin{pmatrix} r & 0 \\ 0 & r+s \end{pmatrix} \quad \text{and} \quad D\mathbf{Y}_{\hat{u}\hat{v}}(q_c) = \begin{pmatrix} r + \frac{r+s}{C-1} & 0 \\ -\frac{(d+r+Mr+Nr)(r+s)}{C-1} & -(r+s) \end{pmatrix},$$

respectively. By means of Hartman-Grobman theorem,¹ it is easy to verify that $\mathbf{0}_{\hat{u}\hat{v}}$ is a hyperbolic repeller and q_c is a hyperbolic saddle. In particular, q_c is attracting along the \hat{v} -axis and has a repelling invariant curve emanating towards the interior of the set $\hat{u} > 0$. The possible scenarios for system (6) are shown in the sketches of Figure 1. The results obtained so far allow us to conclude about the dynamics of (4) at infinity as $x \rightarrow \infty$, but this is not enough to say about the dynamics as $y \rightarrow \infty$. Hence, we now consider the transformation given by

$$(x, y, t) \mapsto \left(\frac{u}{v}, \frac{1}{v}, v^2 t \right), \quad v > 0, u \geq 0. \quad (7)$$

Transformation (7) defines the following system:

$$\mathbf{Y}_{uv} : \begin{cases} \dot{u} = u [r(v-u)(u-Mv) - (u+Nv)(1+Su-dv-C)] ; \\ \dot{v} = -v(u+Nv)(Su-dv-C) \end{cases} \quad (8)$$

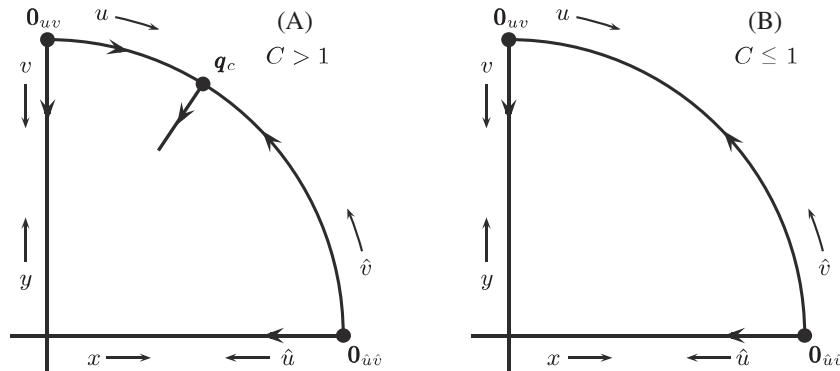


FIGURE 1 Sketches of the local dynamics of the equilibria at infinity (A) for $C > 1$ and (B) for $C \leq 1$

In a similar fashion as with the previous case of (6), orbits of \mathbf{Y} in the limit as $y \rightarrow \infty$ can be studied by investigating the dynamics of \mathbf{Y}_{uv} along the invariant line $v = 0$ with $u \geq 0$. The associated equilibrium points are

$$\mathbf{0}_{uv} = (0, 0), \quad \text{and} \quad \left(\frac{C-1}{r+s}, 0 \right)_{uv} \quad \text{if} \quad C > 1. \quad (9)$$

In particular, the second equilibrium in (9) corresponds to q_C in (6), and, hence, we keep this notation. The associated Jacobian matrix for q_C is

$$D\mathbf{Y}_{uv}(q_C) = \begin{pmatrix} -\frac{(C-1)^2}{r+s} & \frac{(C-1)^2(d+r(1+M+N))}{(r+s)^2} \\ 0 & \frac{(C-1)(Cr+s)}{(r+s)^2} \end{pmatrix}.$$

It follows that q_C is a saddle point of (8). Notice that this is consistent with the analogous result for (6).

On the other hand, the Jacobian matrix associated to $\mathbf{0}_{uv}$ is the null matrix

$$D\mathbf{Y}_{uv}(\mathbf{0}_y) = \begin{pmatrix} 0 & 0 \\ 0 & 0 \end{pmatrix},$$

so we cannot apply Hartman-Grobman theorem. Therefore, we use the blow-up technique⁴³ to get information about the dynamics near $\mathbf{0}_{uv}$. We consider the horizontal blow-up given by the transformation

$$(u, v) \mapsto (x, xy), \quad (10)$$

where, for sake of simplicity, we reuse the variables (x, y) to denote the new coordinates. Notice that this transformation is singular at $\mathbf{0}_{uv}$ since it maps the origin onto the entire line $x = 0$. In addition to (10), we use the time rescaling

$$t \mapsto \frac{t}{x}$$

and obtain the new vector field, denoted as $\tilde{\mathbf{Z}}$, given by

$$\tilde{\mathbf{Z}} : \begin{cases} \dot{x} = x [C(1 + Ny) - x(y - 1)(My - 1)r + (1 + Ny)(dxy - 1 - Sx)] ; \\ \dot{y} = y(1 + Ny + x(y - 1)(My - 1)r). \end{cases}$$

The only equilibrium of $\tilde{\mathbf{Z}}$ in the line $x = 0$ is the origin $\mathbf{0}_{xy} = (0, 0)$, and its Jacobian matrix is

$$D\tilde{\mathbf{Z}}(\mathbf{0}_{xy}) = \begin{pmatrix} C-1 & 0 \\ 0 & 1 \end{pmatrix}.$$

Hence, $\mathbf{0}_{xy} = (0, 0)$ is a hyperbolic saddle of $\tilde{\mathbf{Z}}$ if $C < 1$, and a hyperbolic repeller if $C > 1$ (we remark without showing further calculations that a similar procedure given by a vertical blow-up does not provide additional information). Returning to the system (8) by means of blowing down the axis $x = 0$ back to $\mathbf{0}_{uv}$, one obtains the corresponding local phase portraits of $\mathbf{0}_{uv}$ in Figure 1. Finally, it is straightforward to see from (9) that the case $C = 1$ in (8) corresponds to the collision of $\mathbf{0}_{uv}$ and q_C . From the continuous dependence of solutions of ordinary differential equations with respect to parameter variation,^{1,2} it follows that the local phase portrait at $\mathbf{0}_{uv}$ for $C = 1$ is qualitatively equivalent to that in Figure 1B.

In conclusion, no trajectory of (4) starting in the first quadrant Ω converges to infinity in forward time.

3 | EQUILIBRIUM POINTS

3.1 | Equilibrium points in the axis $y = 0$

System (4) has 3 equilibria in the x -axis, namely, $(0, 0)$, $(M, 0)$, and $(1, 0)$. Their local stabilities are given by the eigenvalues of the corresponding Jacobian matrices. In the case of the origin, the associated Jacobian matrix is

$$DY(0, 0) = \begin{pmatrix} -Mr & 0 \\ 0 & -Nd \end{pmatrix}.$$

Hence, the point $(0, 0)$ is a attracting node. In the case of $(M, 0)$, one obtains

$$DY(M, 0) = \begin{pmatrix} Mr(1 - M) & -M(N + M) \\ 0 & (N + M)(SM - d) \end{pmatrix}.$$

In this case, the eigenvalues are $\lambda_M = (N + M)(SM - d)$ and $\lambda'_M = Mr(1 - M)$. Notice that $\lambda'_M > 0$ since $0 < M < 1$. On the other hand, the sign of λ_M depends on the sign of $SM - d$.

Finally, for $(1, 0)$, we have

$$DY(1, 0) = \begin{pmatrix} r(M - 1) & -(N + 1) \\ 0 & (N + 1)(S - d) \end{pmatrix}$$

with eigenvalues $\lambda_1 = (N + 1)(S - d)$ and $\lambda'_1 = r(M - 1) < 0$.

We can summarise these results in the following lemma.

Lemma 3.1. *The following statements hold in system (4):*

1. *The point $(0, 0)$ is an attracting equilibrium.*
2. *If $d < MS$, the point $(M, 0)$ is a repelling equilibrium, and if $d > MS$, the point $(M, 0)$ is a saddle equilibrium.*
3. *If $d < S$, the point $(1, 0)$ is a saddle equilibrium, and if $d > S$, the point $(1, 0)$ is an attracting equilibrium.*

The transitional cases for both equilibria $(M, 0)$ and $(1, 0)$ correspond to transcritical bifurcations. This is part of the topics explained later in section 4.1.

3.2 | Equilibrium points in $\text{int}(\Omega)$

Let $p = (a, y_a)$ be the coordinates of an equilibrium point in $\text{int}(\Omega)$, ie, the interior of the first quadrant. Hence, by plugging the coordinates y_a and a into (4), we obtain the following algebraic conditions:

$$y_a = \frac{Sa - d}{C} \quad \text{and} \quad r(1 - a)(a - M) - y_a(a + N) = 0. \quad (11)$$

Replacing the second equation of (11) into the first one, we have

$$a^2(Cr + S) + a(SN - d - Cr(M + 1)) + (CrM - dN) = 0. \quad (12)$$

Solutions of this quadratic equation in a are

$$a_+ = \frac{D + \sqrt{\Delta}}{2(Cr + S)} \quad \text{and} \quad a_- = \frac{D - \sqrt{\Delta}}{2(Cr + S)}, \quad (13)$$

provided $\Delta \geq 0$, where

$$\Delta := \Delta(S, d) = (Cr(M + 1) + d - NS)^2 + 4(Cr + S)(dN - CrM) \quad (14)$$

and

$$D = Cr(M + 1) + d - NS.$$

Let us denote $p_+ = (a_+, y_{a_+})$ and $p_- = (a_-, y_{a_-})$ the corresponding points. Before stating the conditions for p_+ and p_- to be in $\text{int}(\Omega)$, let us define the following sets in the parameter plane (S, d) :

$$\mathbf{I} = \{(S, d) \in \mathbb{R}_+^2 \mid d > S\},$$

$$\mathbf{II} = \{(S, d) \in \mathbb{R}_+^2 \mid MS < d < S\},$$

$$\mathbf{III} = \left\{ (S, d) \in \mathbb{R}_+^2 \mid 0 < d < MS, S < \frac{C(1 - M)r}{M + N} \right\} \cap \Delta^{-1}(0, \infty),$$

$$\mathbf{IV} = \mathbb{R}_+^2 \setminus (\mathbf{I} \cup \mathbf{II} \cup \mathbf{III}).$$

Figure 2 shows a sketch of the regions **I** to **IV** and their boundaries in the (S, d) -plane.

Lemma 3.2. *The following statements hold in system (4):*

1. *If $(S, d) \in \mathbf{I} \cup \mathbf{IV}$, there is no equilibrium in $\text{int}(\Omega)$.*
2. *If $(S, d) \in \mathbf{II}$, only the point $p_+ \in \text{int}(\Omega)$.*
3. *If $(S, d) \in \mathbf{III}$, both points $p_+, p_- \in \text{int}(\Omega)$.*

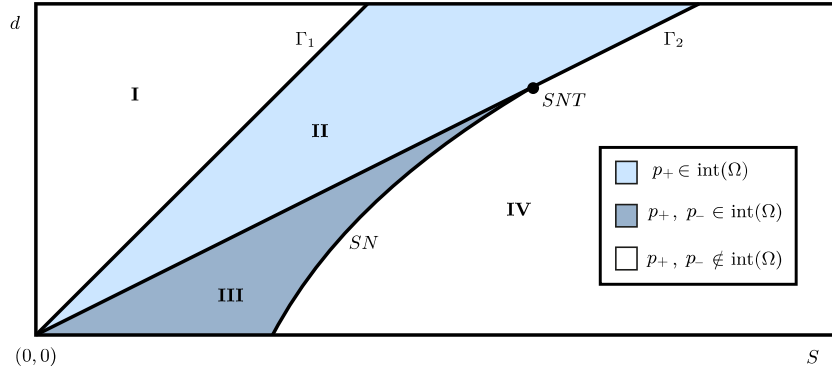


FIGURE 2 Sketches of the curves Γ_1 , Γ_2 , and SN as well as the open regions **I** to **IV** in the (S, d) -plane. The colour code indicates whether p_+ or p_- is in $\text{int}(\Omega)$ [Colour figure can be viewed at wileyonlinelibrary.com]

The proof of Lemma 3.2 is based on the following algebraic arguments. From (13), it is clear that condition $\Delta \geq 0$ is necessary to have equilibrium points in $\text{int}(\Omega)$. Since $d > 0$, the equation $\Delta(S, d) = 0$ in (14) defines implicitly a curve in the (S, d) -plane given as the graph of the function

$$d = \delta(S) := -(Cr(1 + M + 2N) + NS) + 2\sqrt{Cr(1 + N)(M + N)(Cr + S)}, \quad (15)$$

along which there is a single (double) root $a_+ = a_-$. It follows that if $d > \delta(S)$, the discriminant $\Delta > 0$, and so (12) has 2 real roots. In particular, we will prove below that along the curve $d = \delta(S)$, the (double) root is positive—and, hence, the associated equilibrium is in $\text{int}(\Omega)$ —only if $S < \frac{C(1-M)r}{M+N}$. Let us then define the segment of interest as

$$SN = \left\{ (S, d) \in \mathbb{R}_+^2 \mid \Delta(S, d) = 0 \text{ and } S < \frac{C(1-M)r}{M+N} \right\}. \quad (16)$$

Let us now analyse how any equilibrium can enter the set $\text{int}(\Omega)$ by crossing its boundaries. Firstly, from Section 2, no equilibrium can enter (or exit) the interior of the first quadrant through the y -axis. Indeed, the y -axis is an invariant set and its only equilibrium—the origin—is hyperbolic, and, hence, it cannot collide with any other equilibrium. By a similar reasoning, it follows that no equilibrium can bifurcate from infinity towards Ω .

Let us now pay attention to equilibria crossing the x -axis from the fourth to the first quadrant. For $S = 0$ and for every $d \geq 0$, we have $\Delta(0, d) > 0$, and $y_a < 0$ regardless of the sign of a . Hence, in the boundary $S = 0$ in parameter space, there is no equilibria in $\text{int}(\Omega)$ since $y_{a_-} < 0$ and $y_{a_+} < 0$. From (11), the coordinate y_a changes sign only if $d = S$ (with $a = 1$) or $d = MS$ (with $a = M$). Substituting $d = S$ and (13) in the first equation of (11), one obtains the expression

$$y_{a\pm} = -\frac{S(C(1-M)r + S(1+N) \pm |(C(1-M)r + S(1+N))|)}{2C(Cr + S)}.$$

Notice that $S > 0 > \frac{C(M-1)r}{1+N}$, hence $y_{a_+} = 0$, and the point p_+ coincides with $(1, 0)$. By the continuity of the equilibrium coordinates with respect to the parameters, the coordinates $y_{a_+} < 0$ and $y_{a_-} < 0$ for every $(S, d) \in \mathbf{I}$. Hence, as the point (S, d) enters region **II** from region **I** by crossing the straight line

$$\Gamma_1 := \{(S, d) \in \mathbb{R}_+^2 \mid d = S\}, \quad (17)$$

the point p_+ enters the first quadrant in phase space.

Similarly, let us denote

$$\Gamma_2 := \{(S, d) \in \mathbb{R}_+^2 \mid d = MS\}. \quad (18)$$

It is easy to check that the point $(S, d) = \left(\frac{C(1-M)r}{M+N}, M \frac{C(1-M)r}{M+N} \right) \in \Gamma_2$ (denoted as SNT in Figure 2) is a quadratic tangency between Γ_2 and the curve $\Delta(S, d) = 0$. Hence, at SNT , one has $a_+ = a_- = M$, $y_{a_+} = y_{a_-} = 0$ and $\Delta = 0$. Therefore, if $(S, d) = SNT$, both p_+ and p_- coincide with the equilibrium $(M, 0)$. In particular, it follows that the segment SN is qualitatively as in Figure 2.

Substituting $d = MS$ and (13) in the first equation of (11), one obtains the expression

$$y_{a\pm} = \frac{S(C(1-M)r - S(M+N) \pm |C(1-M)r - S(M+N)|)}{2C(Cr + S)}.$$

It follows that if $d = MS$ and $S < \frac{C(1-M)r}{M+N}$, then $y_{a-} = 0$ and the point p_- coincides with $(M, 0)$. Hence, from continuity arguments, as the point (S, d) enters region **III** from region **II** by crossing Γ_2 the point p_- enters the first quadrant. In turn, if $d = MS$ and $S > \frac{C(1-M)r}{M+N}$, then $y_{a+} = 0$ and the point p_+ coincides with $(M, 0)$. Hence, as the point (S, d) enters region **IV** by crossing Γ_2 from region **II**, the point p_+ leaves the first quadrant. As a consequence, the segment $\Delta^{-1}(0) \setminus SN$ (not shown in Figure 2) corresponds to equilibria located outside of Ω . This completes the proof of Lemma 3.2.

3.3 | Stability of equilibrium points in $\text{int}(\Omega)$

The trace and determinant of the Jacobian matrix of (4) at an equilibrium (a, y_a) have the form

$$\text{tr}(DY)(a, y_a) = \frac{1}{C}(dN + CdN - CrM + ((2 + C)d + 2C(1 + M)r - (1 + C)NS)a - (3Cr + (2 + C)S)a^2) \quad (19)$$

and

$$\det(DY)(a, y_a) = \frac{1}{C}(N + a)(d - Sa)(dN - CrM + 2(d + Cr(1 + M) - NS)a - 3(Cr + S)a^2), \quad (20)$$

respectively.

Recall that $\det(DY)(a, y_a) = \lambda_1 \lambda_2$, where λ_1 and λ_2 are the eigenvalues of $DY(a, y_a)$. After some algebraic work, one gets that $\det(DY)(a, y_a)$ vanishes if $(S, d) \in \Gamma_1 \cup \Gamma_2 \cup \Delta^{-1}(0) \cup \Gamma_3$, where

$$\Gamma_3 := \left\{ (S, d) \in \mathbb{R}_+^2 \mid d = \frac{CMr}{N} \right\}.$$

In each of these curves, the matrix $DY(a, y_a)$ has a vanishing eigenvalue. It follows from Lemmas 3.1 and 3.2 that $(S, d) \in \Gamma_1 \cup \Gamma_2$ corresponds to transcritical bifurcations occurring at $(1, 0)$ and $(M, 0)$, respectively. Moreover, from (13) and (16), $(S, d) \in SN \subset \Delta^{-1}(0)$ corresponds to a saddle-node bifurcation of equilibria in $\text{int}(\Omega)$. In turn, if $(S, d) \in \Delta^{-1}(0) \setminus SN$, a saddle-node bifurcation occurs for equilibria outside of Ω . Finally, if $(S, d) \in \Gamma_3$, the determinant $\det(DY)(a, y_a) = 0$ for negative coordinates $y_a < 0$. It follows that the sign of $\det(DY)(a, y_a)$ is constant in the open regions **II** and **III**. Hence, choosing representative parameter values $r = 1$, $M = 0.5$, $N = 2.07719$, and $C = 7$, we obtain $\det(DY)(p_+) > 0$ for $(S, d) \in \text{II} \cup \text{III}$, and $\det(DY)(p_-) < 0$ for $(S, d) \in \text{III}$. By the continuous dependence of $\det(DY)$ with respect to the parameters, the point p_+ is a node or focus, and p_- is a saddle.

On the other hand, let us define the function

$$H(S, d) = dN + CdN - CrM + ((2 + C)d + 2C(1 + M)r - (1 + C)NS)a_+ - (3Cr + (2 + C)S)a_+^2, \quad (21)$$

where a_+ is the x -coordinate of p_+ defined in (13). Hence, from (19), we have $\text{tr}(DY)(p_+) = \frac{H(S, d)}{C}$.

The Hartman-Grobman theorem allows us to summarise the findings in this subsection in the following way:

Theorem 3.3. *The following statements hold in system (4):*

1. *If $(S, d) \in \text{III}$, the point p_- is a saddle equilibrium.*
2. *If $(S, d) \in (\text{II} \cup \text{III}) \cap H^{-1}(0, \infty)$, the point p_+ is a repelling equilibrium.*
3. *If $(S, d) \in (\text{II} \cup \text{III}) \cap H^{-1}(-\infty, 0)$, the point p_+ is an attracting equilibrium.*

In the next section, we will see that equation $H(S, d) = 0$ defines a curve of Hopf bifurcation—not shown in Figure 2—at the equilibrium p_+ . This Hopf bifurcation curve is contained in both regions **II** and **III**, crosses the line Γ_2 , and terminates at the intersection with the curve SN . Hence, at this intersection point, we have $\text{tr}(DY)(a, y_a) = 0$ and $DY(a, y_a) = 0$ simultaneously, and the equilibrium has a single (repeated) eigenvalue $\lambda_1 = \lambda_2 = 0$. This is a necessary condition for system (4) to undergo a Bogdanov-Takens bifurcation.^{1,2}

4 | THE BASINS OF ATTRACTION AND CONDITIONS FOR SURVIVAL

The local analysis of equilibria in Section 3 shows the existence of a number of bifurcation phenomena. This section expands the bifurcation analysis to include global phenomena such as homoclinic and heteroclinic connections. By means

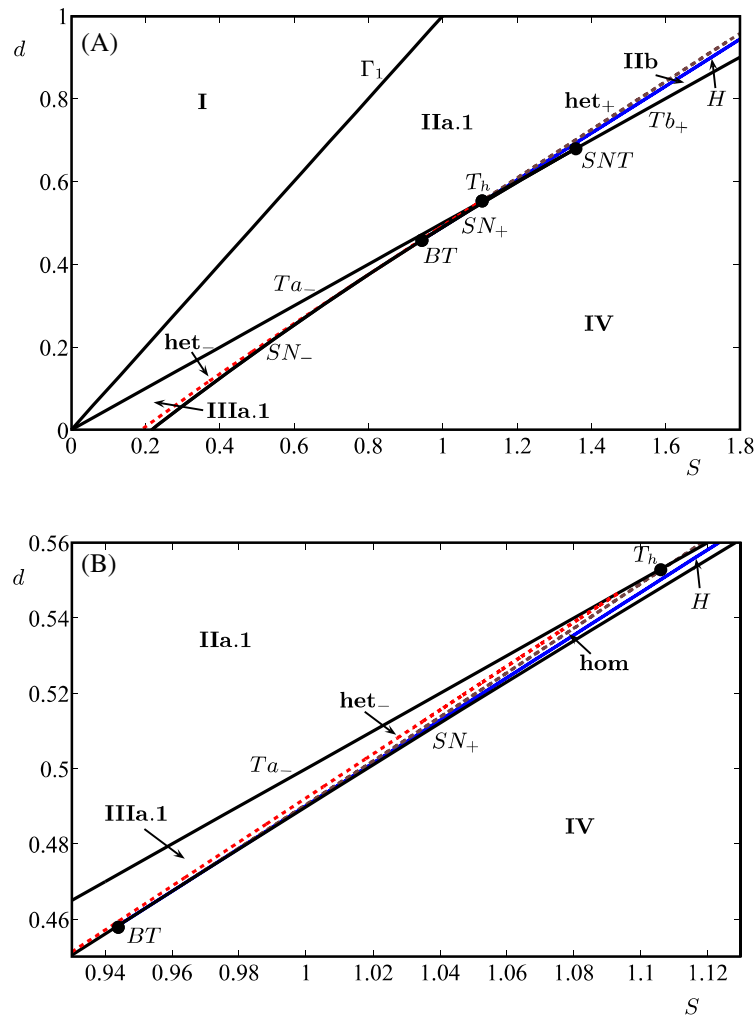


FIGURE 3 (A) The bifurcation diagram of model (4) in the (S, d) -plane obtained by numerical continuation. The (S, d) -plane is partitioned into several open regions divided by curves of saddle-node (SN), transcritical (Γ_1 and $\Gamma_2 := Ta_- \cup Ta_+ \cup Tb_- \cup Tb_+ \cup \{T_h\} \cup \{SNT\}$), Hopf (H), homoclinic (**hom**), and heteroclinic bifurcations (**het**₊ and **het**₋). (B) An enlargement near the Bogdanov-Takens point BT and the point T_h . Parameter values $r = 1$, $M = 0.5$, $N = 2.07719$, and $C = 7$ remain fixed [Colour figure can be viewed at wileyonlinelibrary.com]

of a careful study of the relevant invariant manifolds involved, we also show all the possible phase portraits and basins of the attracting objects.

Today, several computational methods exist to find codimension-1 and -2 bifurcations in vector fields to high accuracy; see Kuznetsov,² Doedel,⁴² and Govaerts⁴⁴ as entry points on the subject. These methods are implemented in standard software packages such as Auto⁴⁵ and Matcont,⁴⁶ which allow one to find bifurcation points numerically and check the corresponding genericity and transversality conditions by monitoring suitable test functions in their routines. In this way, one can detect and continue a bifurcation of interest in parameter space and obtain its unfolding. In what follows, we consider S and d as the continuation parameters—and keep $r = 1$, $M = 0.5$, $N = 2.07719$, and $C = 7$ fixed throughout—and perform a bifurcation analysis with Auto.

Figure 3A shows the bifurcation diagram of (4) in the (S, d) -plane. Figure 3B shows an enlarged region of the same diagram to better distinguish the different bifurcation curves from one another. An accompanying topological sketch of the same bifurcation diagram is shown in Figure 4. For better visualisation of the color in the figures, in what follows we refer the reader to the online version of this paper.

4.1 | The bifurcation diagram

All the bifurcation curves detected analytically in Section 3 are also found numerically and shown in Figures 3 and 4. In particular, the corresponding notation is also kept accordingly. For the sake of completeness, let us start by summarising the local bifurcations. The curve labelled as SN corresponds to a saddle-node bifurcation defined analytically in (16);

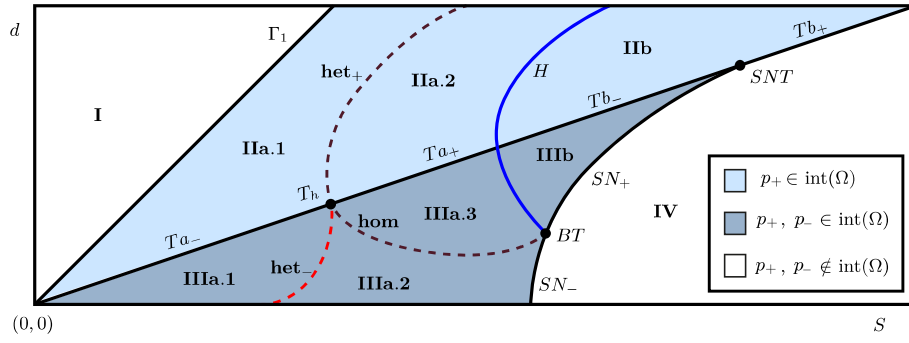


FIGURE 4 Topological sketch of the bifurcation diagram of system (4) in the (S, d) -plane obtained from the analysis in Section 3 and Figure 3 [Colour figure can be viewed at wileyonlinelibrary.com]

hence, for any $(S, d) \in SN$, the equilibria p_- and p_+ coincide. A curve of Hopf bifurcation at p_+ —labelled as H and defined by (21)—intersects the curve SN at a Bogdanov-Takens point BT .

Similarly, the curve Γ_1 corresponds to a transcritical bifurcation defined by (17). More precisely, if (S, d) crosses the curve Γ_1 , the equilibrium p_+ moves from the first to the fourth quadrant of the (x, y) -plane (or vice versa) through the equilibrium $(1, 0)$. The curve

$$\Gamma_2 = Ta_- \cup Ta_+ \cup Tb_- \cup Tb_+ \cup \{T_h\} \cup \{SNT\},$$

defined originally in (18), is formed by the segments in Ta_- , Ta_+ , Tb_- , and Tb_+ . From the analysis in section 3.2, each one of these segments corresponds to transcritical bifurcations too: If (S, d) crosses the curve $Ta_- \cup Ta_+ \cup Tb_- \cup \{T_h\}$, the equilibrium p_- moves from the first to the fourth quadrant of the (S, d) -plane (or vice versa) through the equilibrium $(M, 0)$; in turn, if (S, d) crosses the segment Tb_+ , the equilibria involved at the transcritical bifurcation are p_+ and $(M, 0)$. The transition occurs at the point labelled as $SNT \in \Gamma_2 \cap SN$, which is also the endpoint of the saddle-node curve SN . At $(S, d) = SNT$, the 3 equilibria p_- , p_+ , and $(M, 0)$ effectively coincide in a single point.

Figures 3 and 4 also include 3 curves of global bifurcations. In general, these curves cannot be found analytically—certainly, not by a standard study of eigenvalues—and have to be detected and calculated with advanced computational tools. A curve of homoclinic bifurcation labelled as **hom** emanates from the BT point. For any $(S, d) \in \mathbf{hom}$, there is a homoclinic orbit to the saddle point p_- enclosing the point p_+ . The curve **hom** terminates at the point $T_h \in \Gamma_2$. On the other hand, the segment labelled as **het**₊ corresponds to the formation of a heteroclinic cycle between $(M, 0)$ and $(1, 0)$. The curve **het**₊ can be seen as the continuation of the homoclinic bifurcation curve **hom** past the transcritical bifurcation at $(S, d) = T_h$. A third curve, labelled as **het**₋, emanates from T_h and corresponds to a heteroclinic bifurcation involving p_- and $(1, 0)$.

4.2 | Phase portraits, separatrices, and basins of attraction

All in all, the bifurcation curves in Figures 3 and 4 divide the first quadrant of the (S, d) -plane into several open regions. The phase portrait of (4) changes qualitatively only if the parameter values (S, d) move from one of these open sets into a different one by crossing a bifurcation curve. In turn, the qualitative behaviour of (4) remains topologically unchanged if the variation of (S, d) does not involve trespassing to a different region in the (S, d) -plane. In the following descriptions, $\epsilon > 0$ denotes a sufficiently small number.

Figure 5 shows representative phase portraits for the dynamics of (4) when $(S, d) \in \mathbf{I}$ (panel A); $(S, d) \in \mathbf{IIa.1}$ (panel B); $(S, d) \in \mathbf{IIa.2}$ (panel C) and $(S, d) \in \mathbf{IIb}$ (panel D). We take advantage of the stable manifold theorem,^{1,2} which states that $W^s(M, 0)$ is tangent at $(M, 0)$ to the linear eigenspace $E^s(M, 0)$. Hence, we approximate $W^s(M, 0)$ by the orbit that starts (in backwards time) from an initial point in $E^s(M, 0)$ at a sufficiently small distance δ from the equilibrium $(M, 0)$. Moreover, this orbit lies in an $O(\delta^2)$ -neighbourhood of $W^s(M, 0)$. In our case, we consider $\delta = 10^{-5}$.

In Figure 5, the colour code indicates the different basins of attraction in phase space. The basin of the origin $B(0, 0)$ is white, the grey region corresponds to $B(1, 0)$, and the purple region is $B(p_+)$. Figure 5 is useful in that it clearly shows all the subdivisions of basins of attraction and their associated boundaries. For instance, in regions **I** and **IIa.1**, the manifold $W^s(M, 0)$ emerges as the separatrix of $B(0, 0)$; in region **IIa.2**, the boundary is an unstable limit cycle (red curve in Figure 5C); and in region **IIb**, the only attractor is the origin, and, hence, $B(0, 0)$ is bounded only by the coordinate axes. However, the question of how these basins and separatrices are extended in phase plane for larger values of both

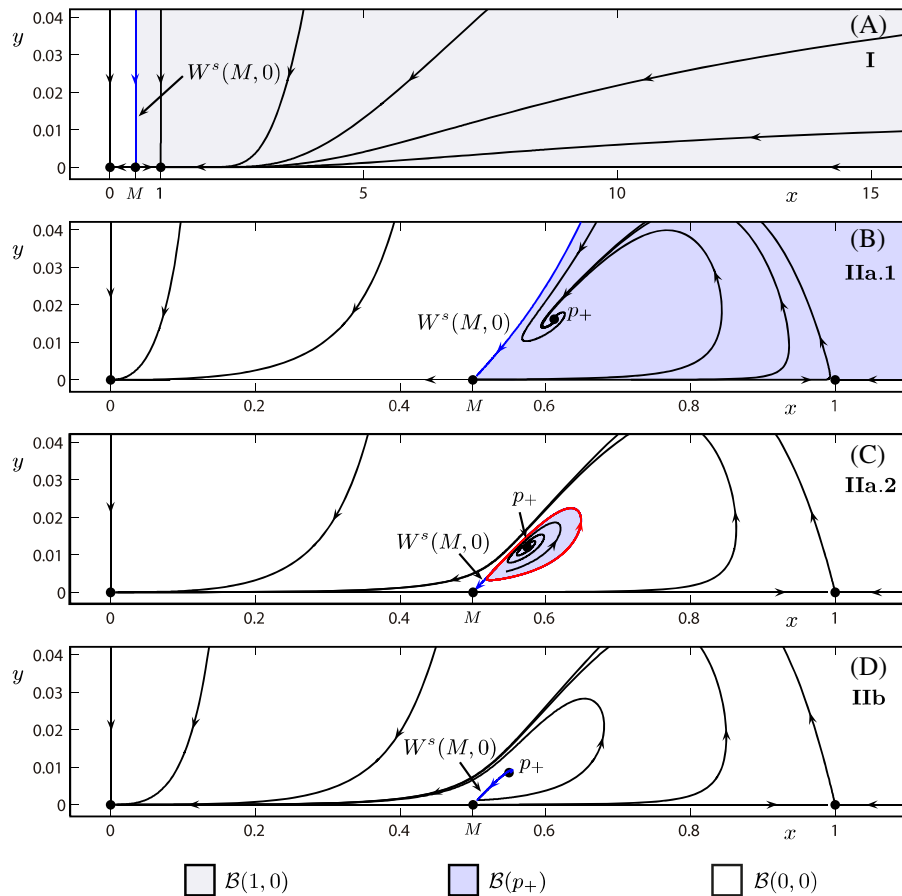


FIGURE 5 Phase portraits of (4) for (A) $(S, d) = (0.4, 0.8) \in \mathbf{I}$; (B) $(S, d) = (1.0674, 0.5384) \in \mathbf{IIa.1}$; (C) $(S, d) = (1.2773, 0.65) \in \mathbf{IIa.2}$; and (D) $(S, d) = (1.3073, 0.66) \in \mathbf{IIb}$. The colour code indicates the different basins of attraction in phase space [Colour figure can be viewed at wileyonlinelibrary.com]

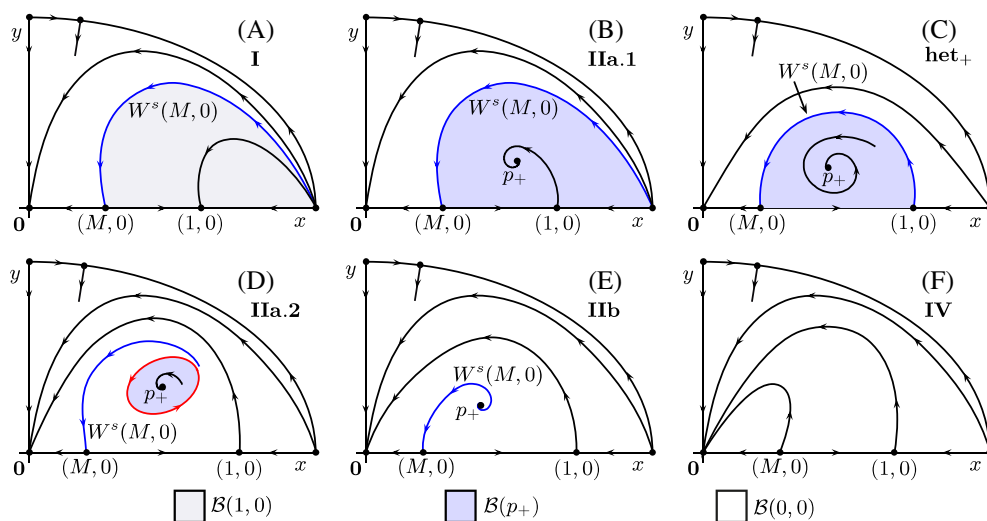


FIGURE 6 Topological sketches of the different phase portraits in the compactification of (4) and basins of attraction when (A) $(S, d) \in \mathbf{I}$; (B) $(S, d) \in \mathbf{IIa.1}$; (C) $(S, d) \in \mathbf{het}_+$; (D) $(S, d) \in \mathbf{IIa.2}$; (E) $(S, d) \in \mathbf{IIb}$; and (F) $(S, d) \in \mathbf{IV}$ [Colour figure can be viewed at wileyonlinelibrary.com]

populations is yet to be answered. Figure 6 shows topological sketches of the different phase portraits of (4) in the compactified first quadrant when $(S, d) \in \mathbf{I}$ (panel A); $(S, d) \in \mathbf{IIa.1}$ (panel B); $(S, d) \in \mathbf{het}_+$ (panel C); $(S, d) \in \mathbf{IIa.2}$ (panel D); $(S, d) \in \mathbf{IIb}$ (panel E); and $(S, d) \in \mathbf{IV}$ (panel F). These topological sketches are the result of incorporating the findings

in Section 2 about the dynamics of (4) at infinity, and a careful analysis of the consequences of the bifurcation phenomena in Figures 3 and 4.

Let us now look at the different portraits, the basins of attraction and their boundaries in more detail. If $d > S$, then $(S, d) \in \mathbf{I}$, and the stable manifold $W^s(M, 0)$ forms the boundary between the basin of attraction of the origin $B(0)$ and the basin $B(1, 0)$ of the attractor $(1, 0)$. Since there are no other equilibria in Ω , it follows from the analysis in Section 2 that $W^s(M, 0)$ extends itself (in backward time) up to infinity. We will prove below that, in our scenario, $W^s(M, 0)$ has to stretch up to the equilibrium at infinity located at $y = 0$ as $x \rightarrow \infty$; see Figure 6A. If $d = S$, then $(S, d) \in \Gamma_1$, and the phase portrait (not shown) is qualitatively as in Figure 6A. In Figure 6B, if $d = S - \epsilon$ and $(S, d) \in \mathbf{IIa.1}$, an attracting equilibrium p_+ is in the first quadrant. The basin of attraction $B(p_+)$ can be seen as the continuation of $B(1, 0)$ after the transcritical bifurcation at Γ_1 when $d = S$; in this case, $W^s(M, 0)$ forms the boundary between $B(p_+)$ and $B(0)$. Since $W^s(M, 0)$ converges to infinity when extended backwards in time, the basin $B(p_+)$ is unbounded. As (S, d) moves towards the curve **het** from region **IIa.1**, the separatrix $W^s(M, 0)$ approaches the saddle point $(1, 0)$. In the limit when $(S, d) \in \mathbf{het}$, in Figure 6C, the stable manifold $W^s(M, 0)$ joins the equilibrium $(1, 0)$ to form a heteroclinic cycle. Simultaneously, the basin $B(p_+)$ becomes a bounded set. As (S, d) enters the region **IIa.2** by crossing the curve **het**, in Figure 6D, an unstable limit cycle bifurcates. The formation of the heteroclinic cycle in Figure 6C is the consequence of a transverse intersection of $W^s(M, 0)$ and the 1-dimensional unstable manifold $W^u(1, 0)$ of $(1, 0)$. Indeed, as the parameter (S, d) crosses the curve **het** from regions **IIa.1** to **IIa.2** (or vice versa), both invariant manifolds interchange their relative positions. From the flow box theorem,⁴³ it follows that the intersection of $W^s(M, 0)$ and $W^s(1, 0)$ is possible only if, for $(S, d) \in \mathbf{IIa.1}$, $W^s(M, 0)$ extends itself to the equilibrium at infinity located at $y = 0$ as $x \rightarrow \infty$. From the smooth dependence of the flow under parameter variation, the same statement on $W^s(M, 0)$ holds in region **I**.

The periodic orbit in Figure 6D forms the basin boundary of the attractor p_+ . This unstable limit cycle disappears at a subcritical Hopf bifurcation when $(S, d) \in \mathbf{H}$ so that, if $(S, d) \in \mathbf{IIb}$, in Figure 6E, the equilibrium p_- is now a repeller. Finally, in Figure 6F, if (S, d) enters the region **IV** by crossing the segment Tb_+ , the point p_- moves to the fourth quadrant, and no equilibrium remains in the interior of the first quadrant; the only attractor of the system is the origin. In particular, the phase portrait if $(S, d) \in Tb_+$ is qualitatively as in Figure 6F.

Similarly, Figure 7 shows topological sketches of the different phase portraits of (4) when $(S, d) \in \mathbf{IIIa.1}$ (panel A); $(S, d) \in \mathbf{het_-}$ (panel B); $(S, d) \in \mathbf{IIIa.2}$ (panel C); $(S, d) \in \mathbf{hom}$ (panel D); $(S, d) \in \mathbf{IIIa.3}$ (panel E); and $(S, d) \in \mathbf{IIIb}$ (panel F). In Figure 7A, when $(S, d) \in \mathbf{IIIa.1}$, the equilibrium p_+ is an attractor—as in region **IIa.1**, compare with Figure 6B—but now, it is also accompanied in Ω by the saddle point p_- . The stable manifold $W^s(p_-)$ separates $B(p_+)$ and $B(0)$ from one another, and both basins are unbounded. If $(S, d) \in \mathbf{het_-}$, in Figure 7B, the upper branch of $W^s(p_-)$ forms a heteroclinic connection between p_- and $(1, 0)$; this forces $B(p_+)$ to become a bounded set much as in the heteroclinic transition at **het**, compare with Figure 6C. As (S, d) crosses **het_-** into the region **IIIa.2** in Figure 7C, the heteroclinic connection is broken. In particular, from analogous reasons as those stated for region **I**, it follows that in region **IIIa.1**, the stable manifold

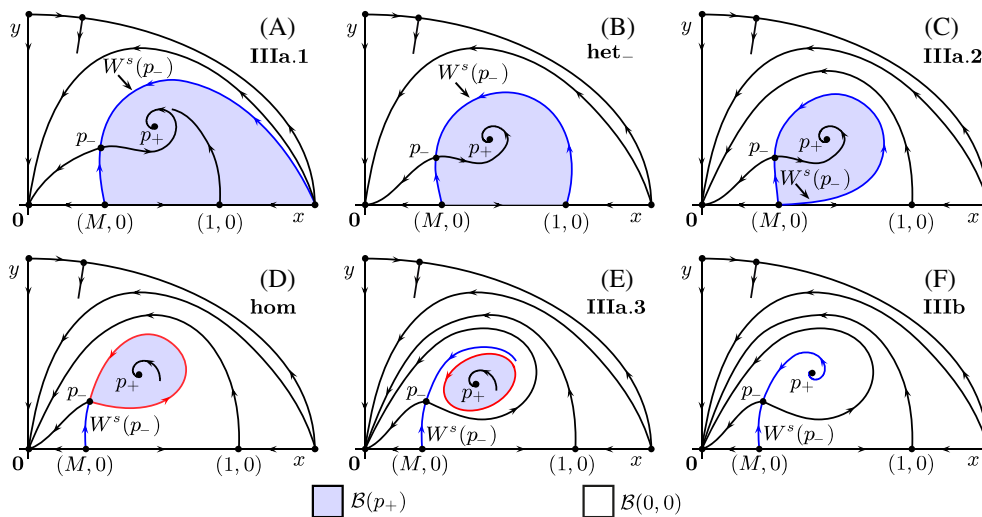


FIGURE 7 Topological sketches of the different phase portraits in the compactification of (4) and basins of attraction when (A) $(S, d) \in \mathbf{IIIa.1}$; (B) $(S, d) \in \mathbf{het_-}$; (C) $(S, d) \in \mathbf{IIIa.2}$; (D) $(S, d) \in \mathbf{hom}$; (E) $(S, d) \in \mathbf{IIIa.3}$; and (F) $(S, d) \in \mathbf{IIIb}$ [Colour figure can be viewed at wileyonlinelibrary.com]

$W^s(p_-)$ converges (in backwards time) to the equilibrium at infinity located at $y = 0$ as $x \rightarrow \infty$.) As (S, d) approaches the curve **hom** and the upper branch of $W^s(p_-)$ moves closer to the right-hand side of $W^u(p_-)$, the area of the basin $B(p_+)$ is reduced. In the limit, when $(S, d) \in \mathbf{hom}$ in Figure 7D, a homoclinic orbit to p_- becomes the basin boundary of the attractor p_+ . Consequently, if (S, d) crosses towards the region **IIIa.3** in Figure 7E, an unstable limit cycle bifurcates and becomes the boundary of $B(p_+)$. Finally, in Figure 7F, this cycle disappears at a subcritical Hopf bifurcation when (S, d) crosses the curve **hom** towards the region **IIb**.

For the sake of completeness, from the continuous dependence of the dynamics with respect to parameter variation, it is easy to verify that the phase portrait corresponding to the segment **Ta₋** is qualitatively as in Figure 6B. Likewise, the phase portrait corresponding to the segment **Tb₋** is qualitatively as in Figure 6E; the phase portrait corresponding to the segment **Tb₊** is qualitatively as in Figure 6F, and the phase portrait corresponding to the point T_h is qualitatively as in Figure 6C. On the other hand, if $(S, d) \in SN_- \cup SN_+$, the points $p_+ = p_-$ coincide as a partially hyperbolic equilibrium. If $(S, d) \in SN_-$, this equilibrium has a 1-dimensional stable manifold $W^s(p_+)$ that separates the basins $B(p_+)$ and $B(0, 0)$.

Figures 6 and 7 are also useful to determine the possible scenarios of survival and coexistence. For instance, long-term survival of both species may occur only if parameters (S, d) are in those sets, where p_+ exists and has a basin of attraction, ie, if $(S, d) \in \mathbf{IIa.1} \cup \mathbf{het}_+ \cup \mathbf{Ta}_- \cup \{T_h\} \cup \mathbf{IIIa.1} \cup \mathbf{het}_- \cup \mathbf{IIIa.2} \cup \mathbf{hom} \cup \mathbf{IIIa.3}$. In all these cases, the Allee threshold is the common boundary between $B(0, 0)$ and $B(p_+)$. This fact highlights how relevant it is to find the basin boundaries of $B(p_+)$ to determine conditions for coexistence. Another type of long-term situation may occur if $(S, d) \in \mathbf{IIb} \cup \mathbf{IIIb} \cup \mathbf{IV}$. In this case, any generic orbit in Ω converges to the origin leading to the extinction of both species; the exception is $W^s(M, 0)$ in regions **IIb** and **IIIb**. Hence, if $(S, d) \in \mathbf{IIb} \cup \mathbf{IIIb} \cup \mathbf{IV}$, there is no Allee threshold in $\text{int}(\Omega)$. The final scenario occurs if $(S, d) \in \mathbf{I}$: An initial condition in $B(1, 0)$ leads to the long-term survival of the prey species and the extinction of the predators.

Notice that the numerical routines implemented in Auto to check nondegeneracies in bifurcations allow us to extend our findings to an open set of parameters around those that we have considered; see also Doedel.⁴² This enables us to summarise our results as follows:

Result 1. *There is an open set of parameter values around $(r, M, N, C) = (1, 0.5, 2.07719, 7)$ such that the bifurcation diagram of (4) is topologically equivalent to those in Figures 3 and 4. Furthermore, the Allee threshold in $\text{int}(\Omega)$ satisfies:*

1. *If $(S, d) \in \mathbf{I} \cup \Gamma_1$, the Allee threshold is the common boundary between $B(0, 0)$ and $B(1, 0)$. Moreover, it corresponds to the stable manifold $W^s(M, 0)$ of the point $(M, 0)$.*
2. *If $(S, d) \in \mathbf{IIa.1} \cup \mathbf{het}_+ \cup \mathbf{Ta}_- \cup \{T_h\} \cup \mathbf{IIIa.1} \cup \mathbf{het}_- \cup \mathbf{IIIa.2} \cup \mathbf{IIa.2} \cup \mathbf{hom} \cup \mathbf{IIIa.3} \cup SN_-$, the Allee threshold is the common boundary between $B(0, 0)$ and $B(p_+)$. Moreover,*
 - (a) *if $(S, d) \in \mathbf{IIa.1} \cup \mathbf{het}_+ \cup \mathbf{Ta}_- \cup \{T_h\}$, the Allee threshold corresponds to the stable manifold $W^s(M, 0)$ of the point $(M, 0)$;*
 - (b) *if $(S, d) \in \mathbf{IIIa.1} \cup \mathbf{het}_- \cup \mathbf{IIIa.2}$, the Allee threshold corresponds to the stable manifold $W^s(p_-)$ of the point p_- ;*
 - (c) *if $(S, d) \in \mathbf{IIa.2} \cup \mathbf{IIIa.3}$, the Allee threshold corresponds to an unstable limit cycle which surrounds p_+ ;*
 - (d) *if $(S, d) \in \mathbf{hom}$, the Allee threshold corresponds to a homoclinic orbit to the saddle point p_- ;*
 - (e) *if $(S, d) \in SN_-$, the Allee threshold corresponds to the stable manifold $W^s(p_+)$ of the partially hyperbolic equilibrium $p_+ = p_-$.*

5 | DISCUSSION

We have investigated the nature of Allee thresholds and basins of attraction in a predation model. The main feature of the model is that a double Allee effect is present in the prey species. In addition, the predator population shows a competition behaviour. All the analysis has been performed on a qualitatively equivalent system, which was obtained by means of a suitable change of coordinates and time rescaling and an invertible reparameterization. We prove that the model is well-posed in the sense that every trajectory starting from a realistic initial condition remains bounded in the first quadrant Ω . This result was obtained by showing that the coordinate axes are invariant and by studying the behaviour at infinity by means of a Poincaré compactification. In particular, we made use of the blow-up technique to desingularise equilibrium points at infinity and prove that no (realistic) orbit can converge to infinity.

Our model can have up to 5 equilibrium points in the first quadrant. The origin $(0, 0)$ is always an attracting equilibrium, which prompts the chance of extinction of both populations. The point $(M, 0)$ is also always an equilibrium. Here, $0 < M = \frac{m}{k} < 1$ is a rescaled Allee parameter; M measures the proportion of the original Allee parameter m over the carrying capacity k . Our findings show that the equilibrium $(M, 0)$ is a repeller if $d - ms < 0$; in this case, the predator mortality rate d is smaller than the product of m and the predator's competition rate s . In the opposite case, ie, $d - ms > 0$, the point $(M, 0)$ is a saddle equilibrium. On the other hand, the point $(1, 0)$ is a saddle if $d < sk$. Hence, if the predator mortality rate d is smaller than the product between the predator growth rate s and the prey carrying capacity, the equilibrium $(1, 0)$ is unstable.

The 2 other equilibria p_+ and p_- correspond to asymptotic states with positive coordinates. We found analytical conditions for these equilibria to exist in the interior of the first quadrant. Furthermore, we give a geometric representation of these algebraic conditions that tells us how many positive equilibria the system allows depending on the values of parameters d and $S = sk$. More concretely, the (S, d) plane is divided into 4 regions, **I** to **IV**. If $(S, d) \in \mathbf{I} \cap \mathbf{IV}$, the system has no positive equilibrium; in region **II**, we have p_+ only; and in region **III**, we have both p_+ and p_- . Moreover, the boundary between regions **III** and **IV** determines a curve of saddle-node bifurcation. On the other hand, the boundary between **I** and **II** is a transcritical bifurcation curve (as well as the boundaries between **II** and **III**, and between **II** and **IV**). The local stability of the equilibria p_+ and p_- is also described: for instance, in region **III**, the point p_- is a saddle equilibrium. In turn, the point p_+ changes stability at a curve of Hopf bifurcation H that is contained in regions **II** and **III**. It is an interesting realisation that all these analytical conditions for existence and stability of positive equilibria involve algebraic expressions that depend on all parameters. In particular, the parameter n —corresponding to the second Allee effect on the prey—appears explicitly in its rescaled form $N = \frac{n}{k}$, ie, as the ratio between n and the prey carrying capacity.

All these analytical results are combined with a numerical bifurcation analysis performed in the continuation package Auto.⁴⁵ This allows us to obtain a full bifurcation diagram showing both local and global phenomena in Figures 3 and 4. In particular, we identify 3 codimension-2 points that act as organising centres for the dynamics. The first one is a Bogdanov-Takens point on the curve of saddle-node bifurcation (a homoclinic bifurcation curve **hom** emanates from this Bogdanov-Takens point). The second codimension-2 point is a transcritical heteroclinic point T_h : This point is effectively the meeting point of 4 bifurcation curves: the transcritical bifurcation curve, the curve **hom**, a curve of heteroclinic bifurcation in region **III**, and a curve of heteroclinic bifurcation in region **II**. The third organising point (denoted as SNT) indicates the simultaneous occurrence of a saddle-node bifurcation between p_- and p_+ and a transcritical bifurcation at $(M, 0)$ in which is, effectively, a collision of 3 equilibria on the x -axis.

The bifurcation analysis (combined with our knowledge of the dynamics at infinity) allows us to identify the mathematical mechanisms that produce a reorganisation of phase space. Indeed, an analysis of the invariant manifolds in the first quadrant reveals how the basins of attraction rearrange themselves under parameter variation. More concretely, we identify all the basins of attraction in Ω and 3 possible scenarios for the Allee threshold. Namely, the basin boundary of the origin (ie, the extinction equilibrium) may correspond either (1) to the stable manifold of a distinguished saddle equilibrium, (2) to a limit cycle, or (3) to a homoclinic orbit. This is one of the highlights of this work, ie, by means of analytical and geometrical criteria, to be able to determine the possible ecological scenarios of survival, coexistence, or extinction of the 2 populations depending on the values of the model parameters. For instance, in case 1, the initial state of the populations has to be beyond the 1-dimensional stable manifold to avoid extinction and converge to the equilibrium p_+ . In case 2, there is an (unstable) asymptotic periodic state—both populations oscillating in time—that serves as the survival threshold. Finally, in the third scenario, the Allee threshold is, effectively, a solution that converges to the equilibrium p_- in both forward and backward time.

Notice that our description of basin boundaries is also consistent. Indeed, consider any closed path in the (S, d) -plane in Figures 3 and 4 and choose an arbitrary initial point in this path from which (S, d) starts to move; then, regardless of what bifurcation curves the point (S, d) crosses along this path, the resulting phase portraits at the start and at the end of the circuit are always the same. Furthermore, while some bifurcation curves have been found numerically, our bifurcation diagram is minimal in the sense that no extra bifurcation is needed to explain the transition(s) between any 2 phase portraits. Hence, the long-term behaviour of the populations and its dependence on the model parameters can be fully understood from Figures 3 and 4.

Finally, notice that this work is also useful in that it shows the scope of what can be achieved in population dynamics with a combination of bifurcation theory, advanced numerical techniques for dynamical systems, and invariant manifold analysis; see also Aguirre et al³⁻⁶ as other examples of this modern blend of diverse tools. For instance, similar techniques are currently being applied by one of these authors to study a similar model with double Allee effect and a Leslie-Gower type of approach for the conversion rate of captured preys into births of new predators.^{31,35}

ACKNOWLEDGEMENTS

P.A. was partially funded by CONICYT-FONDECYT grant No. 11150306 and Proyecto Basal CMM Universidad de Chile.

ORCID

Pablo Aguirre  <http://orcid.org/0000-0001-6206-370X>

REFERENCES

1. Guckenheimer J, Holmes P. *Nonlinear Oscillations, Dynamical Systems, and Bifurcations of Vector Fields*. 2nd. New York, Springer; 1986.
2. Kuznetsov YA. *Elements of Applied Bifurcation Theory*, 3rd ed. New York: Springer; 2004.
3. Aguirre P. Bifurcations of two-dimensional global invariant manifolds near a non-central saddle-node homoclinic orbit. *SIAM J Appl Dyn Syst*. 2015;14(3):1600-1644.
4. Aguirre P, Krauskopf B, Osinga HM. Global invariant manifolds near homoclinic orbits to a real saddle: (non)orientability and flip bifurcation. *SIAM J Appl Dyn Syst*. 2013;12(4):1803-1846.
5. Aguirre P, Krauskopf B, Osinga HM. Global invariant manifolds near a Shilnikov homoclinic bifurcation. *J Comput Dyn*. 2014;1(1):1-38.
6. Aguirre P, Flores JD, González-Olivares E. Bifurcations and global dynamics in a predator-prey model with a strong Allee effect on the prey, and a ratio-dependent functional response. *Nonlinear Anal Real World Appl*. 2013;16:235-249.
7. Allee WC. *Animal Aggregations, A Study in General Sociology*. Chicago: University of Chicago Press; 1931.
8. Kramer AM, Dennis B, Liebhold AM, Drake JM. The evidence for Allee effects. *Popul Ecol*. 2009;51(3):341-354.
9. Lidicker Jr WZ. The Allee effect: its history and future importance. *Open Ecol J*. 2010;3:71-82.
10. Cai Y, Banerjee M, Kang Y, Wang W. Spatiotemporal complexity in a predator-prey model with weak Allee effects. *Math Biosci Eng*. 2014;11:1247-1274.
11. Bazykin AD. *Nonlinear Dynamics of Interacting Populations*, World Scientific Series on Nonlinear Science Series A, vol. 11. London: World Scientific Publishing Co; 1998.
12. Murray JD. *Mathematical Biology I: An Introduction*, 3rd. New York: Springer-Verlag; 2002.
13. Cai Y, Zhao C, Wang W, Wang J. Dynamics of a Leslie-Gower predator-prey model with additive Allee effect. *Appl Math Modell*. 2015;35:2092-2106.
14. Bascompte J. Extinction thresholds: insights from simple models. *Ann Zool Fennici*. 2003;40(2):99-114.
15. Clark CW. *Mathematical Bioeconomic. The Optimal Management of Renewable Resources*. Indianapolis: Wiley-Interscience; 1990.
16. Stephens PA, Sutherland WJ. Consequences of the Allee effect for behaviour, ecology and conservation. *Trends in Ecol*. 1999;14(10):401-405.
17. Berec L, Angulo E, Courchamp F. Multiple Allee effects and population management. *Trends Ecol Evolut*. 2007;22(4):185-191.
18. De Roos AM, Persson L. Size-dependent life-history traits promote catastrophic collapses of top predators. *PNAS*. 2002;99(20):12907-12912.
19. Clark CW. *The Worldwide Crisis in Fisheries: Economic Models and Human Behavior*. Cambridge: Cambridge University Press; 2006.
20. Courchamp F, Grenfell BT, Clutton-Brock TH. Impact of natural enemies on obligately cooperative breeders. *Oikos*. 2000;91(2):311-322.
21. Gascoigne J, Lipcius RN. Allee effects driven by predation. *J Appl Ecol*. 2004;41(5):801-810.
22. Gregory S, Courchamp F. Safety in numbers: extinction arising from predator-driven Allee effects. *J Anim Ecol*. 2010;79(3):511-514.
23. Kramer AM, Drake JM. Experimental demonstration of population extinction due to a predator-driven Allee effect. *J Anim Ecol*. 2010;79(3):633-639.
24. Freedman HI, Wolkowicz GSK. Predator-prey systems with group defense: the paradox of enrichment revisited. *Bull Math Biol*. 1986;8(5):493-508.
25. Ruan S, Xiao D. Global analysis in a predator-prey system with nonmonotonic functional response. *SIAM J Appl Math*. 2001;61(4):1445-1472.
26. Wolkowicz GSW. Bifurcation analysis of a predator-prey system involving group defense. *SIAM J Appl Math*. 1988;48(3):592-606.
27. Xiao D, Ruan S. Codimension two bifurcations in a predator-prey system with group defense. *Int J Bifurcation Chaos*. 2001;11(8):2123-2131.
28. Angulo E, Roemer GW, Berec L, Gascoigne J, Courchamp F. Double Allee effects and extinction in the Island Fox. *Conserv Biol*. 2007;21(4):1082-1091.
29. González-Olivares E, González-Yáñez B, Mena-Lorca J, Rojas-Palma A, Flores JD. Consequences of double Allee effect on the number of limit cycles in a predator-prey model. *Comput Math Appl*. 2011;62(9):3449-3463.
30. Boukal DS, Berec L. Single-species models of the Allee effect: extinction boundaries, sex ratios and mate encounters. *J Theor Biol*. 2002;218(3):375-394.
31. Aguirre P. A general class of predation models with multiplicative Allee effect. *Nonlinear Dyn*. 2014;78(1):629-648.
32. Barclay H, Mackauer M. The sterile insect release method for pest control: a density-dependent model. *Environ Entomol*. 1980;9(6):810-817.

33. González-Olivares E, Huincahue-Arcos J. Double Allee effects on prey in a modified Rosenzweig-MacArthur predator-prey model. In: Mastorakis N, Mladenov V, Eds. *Computational Problems in Engineering*, Lecture Notes in Electrical Engineering, vol. 307. Basel: Springer International Publishing; 2014:105-119.
34. Stephens PA, Sutherland WJ, Freckleton RP. What is the Allee effect? *Oikos*. 1999;87(1):185-190.
35. Aguirre P, González-Olivares E, Sáez E. Three limit cycles in a Leslie-Gower predator-prey model with additive Allee effect. *SIAM J Appl Math*. 2009;69(5):1244-1262.
36. González-Olivares E, Gallego-Berrio LM, González-Yáñez B, Rojas-Palma A. Consequences of weak Allee effect on prey in the May-Holling-Tanner predator-prey model. *Math Meth Appl Sci*. 2015;38(18):5183-5196.
37. González-Olivares E, Rojas-Palma A. Multiple limit cycles in a Gause type predator-prey model with Holling type III functional response and Allee effect on prey. *Bull Math Biol*. 2011;73(6):1378-1397.
38. González-Olivares E, Rojas-Palma A. Limit cycles in a Gause-type predator-prey model with sigmoid functional response and weak Allee effect on prey. *Math Meth Appl Sci*. 2012;35(8):963-975.
39. López-Ruiz R, Fournier-Prunaret D. Indirect Allee effect, bistability and chaotic oscillations in a predator-prey discrete model of logistic type. *Chaos Solitons Fractals*. 2005;24(1):85-101.
40. Sen M, Banerjee M, Morozov A. Bifurcation analysis of a ratio-dependent preypredator model with the Allee effect. *Ecol Complex*. 2012;11:12-27.
41. Wang J, Shi J, Wei JJ. Predatorprey system with strong Allee effect in prey. *Math Biol*. 2011;62(3):291-331.
42. Doedel EJ. Lecture notes on numerical analysis of nonlinear equations. In: Krauskopf B, Osinga HM, Galán-Vioque J, Understanding Complex Systems, Eds. *Numerical Continuation Methods for Dynamical Systems*. New York: Springer-Verlag; 2007:1-49.
43. Dumortier F, Llibre J, Artés JC. *Qualitative Theory of Planar Differential Systems*. Berlin Heidelberg: Springer; 2006.
44. Govaerts W. *Numerical Methods for Bifurcations of Dynamical Equilibria*. Philadelphia: SIAM; 2000.
45. Doedel EJ, Champneys AR, Dercole F, et al. *AUTO-07p: Continuation and Bifurcation Software for Ordinary Differential Equations*. Montreal, QC, Canada: Department of Computer Science, Concordia University; 2010.
46. Dhooge A, Govaerts W, Kuznetsov YUA. MATCONT: A Matlab package for numerical bifurcation analysis of ODEs. *ACM Trans Math Software*. 2003;29:141-164.

How to cite this article: Contreras D, Aguirre P. Allee thresholds and basins of attraction in a predation model with double Allee effect. *Math Meth Appl Sci*. 2018;1–16. <https://doi.org/10.1002/mma.4774>